Microscale shaping and rounding of ridge arrays and star pattern features on nickel mould via electrochemical polishing

Sana Zaki[1] · Nan Zhang[1] · Michael D. Gilchrist[1]

Abstract High quality micro mould tools are critical for ensuring defect-free production of micro injection moulded products. The demoulding stage of the micro injection moulding can adversely affect the surface integrity due to friction, adhesion and thermal stresses between the metallic mould and polymeric replicated part. In the present work, we propose the use of precision electropolishing (EP) as a shaping and polishing process to control the draft angle and fillet radius of micro features in order to ease demoulding. Typical defects that occur in replicated polymer parts include cracks, burrs and distorted features. A nickel mould having multiple linear ridges and star shape patterns was designed for the present investigation to have characteristic dimensions ranging from 10 μm to 150 μm and with various aspect ratios to study the effect of electropolishing on modifying the shape of micro features and surface morphology. A transient 2D computational analysis has been conducted to anticipate the effect of shaping on the Ni mould after electrochemical polishing with non-uniform material removal rates, based on the distribution of current density. The experimental results indicate that after shaping using EP, the draft angle of star-patterns and linear patterns can be effectively increased by approximately 3.6°, while the fillet radius increases by up to 5.0 μm. By controlling the electropolishing process, the surface roughness can be maintained under 50 nm. This work uses a green and environmental friendly nickel sulfamate electrolyte which can be effective for shaping of nickel micro features without causing any surface deposition.

Keywords Micro feature shaping and electropolishing · Micro mould tools · Green electrolyte · Demoulding micro patterns

1 Introduction

The quality of a plastic micro replicated surface feature depends strongly on the associated performance of micro mould tools. Micro injection moulding (μ-IM) is a well-established process for mass production of polymeric components having sub-millimeter scale features, such as microfluidics [1], lab on chip [2], drug delivery [3] and textured functionalised surfaces [4]. The functionality of such devices is determined largely by feature accuracy, e.g., without distortions and a smooth surface free from burrs and other defects [5, 6]. Typically, in a micro injection moulding process, molten polymer material flows into the mould cavity to replicate the geometry of the micro structured mould insert and is then ejected out at the end of μ-IM after solidification. Demoulding is an important process to determine the integrity of microstructures, as the softer plastic can be damaged easily when separating from the harder mould. Three kinds of forces are involved in the demoulding process, namely adhesion [7], friction [8] and thermal stresses [9]; these exist due to the contact between a mould tool and polymer part. If these are excessive, they can lead to demoulding defects, e.g., distortion, material pile up and damage [10, 11]. This is more commonly associated with micro-injection moulding given the miniature dimensions and correspondingly high surface to volume ratio, and greater injection pressures involved compared with conventional injection moulding.

✉ Nan Zhang
  nan.zhang@ucd.ie

✉ Michael D. Gilchrist
  michael.gilchrist@ucd.ie

1   School of Mechanical and Materials Engineering, University College Dublin, Belfield, Dublin 4, Ireland

Microfabrication techniques, i.e., micro milling, micro electric discharge machining (EDM) and electrochemical erosion are used to fabricate micro tools [12–14]. Mould tool design parameters are vital to address these demoulding challenges, such as draft angle [15, 16], anti-stick coatings [17], low adhesion [18], hydrophobicity [19] and the presence of a smooth surface [20]. Normally, mould tools have a rectangular profile, particularly for features smaller than 100 μm, due to the limitations of existing microfabrication techniques. This rectangular profile aggravates the demoulding forces leading to micro feature cracks, distortion and poor surface quality. Limited efforts have been made to ease demoulding. Jong et al. [16] created a computer algorithm to generate automatic draft angle for various mould designs to reduce the occurrence of demoulding defects. They used various geometric surfaces, points and curves to identify suitable draft angles to improve the mould design and injection moulding efficiency. In another study, Li et al. [21] used a method to evaluate and decouple the problem of friction and adhesion occurring at the interface of mould tool/polymer in nano photonic structures. Quantitative results showed that the magnitude of friction forces on the sidewalls was far more significant than the adhesion stress on the top and bottom of the features. A combined solution was presented by coating the mould with a conformal Al_2O_3 film through atomic layer deposition (ALD) which decreased the total demoulding force. In a recent study, Schoenherr et al. [15] designed a mould tool with a channel depth and width of 300 μm with a draft angle of 10º for a microfluidic device using micro milling, in an effort to reduce adhesion induced demoulding defects. The functionality of the tool was determined by producing polyethylene terephthalate (PET) specimens via coated and uncoated mould inserts at various temperatures of 40, 50 and 60 ℃; the best result was achieved using a CrN coated mould that provided fewer demoulding defects.

An early review of nanofabrication processes [22] illustrated the use of electroforming to manufacture metallic micro-electromechanical systems (MEMS) structures. Chang et al. [23] used direct current-based etching mechanisms to modify a tungsten tip profile, resulting in non-uniform material removal rates with a faster reaction rate at the depth, which yielded a tip diameter of (4±2) μm. On the other hand, some micro-nano shaping techniques have been used to create unique geometries, including needles and formed micro rods, based on dissolution and etching mechanisms. Chen and Yuan [24] demonstrated the process by which tungsten filaments were partially dissolved in an aqueous potassium hydroxide solution under the action of external electric fields, in which capillary adhesion led to an optimised final tip shape.

Inspired by this prior work, we have proposed a solution to minimise or avoid the occurrence of demoulding defects, by shaping and rounding of micro mould tools, i.e., increasing the fillet radius and draft angle [25] which can improve the ultimate performance of μ-IM tools. As seen in Fig. 1, it is seen clearly that a rectangular cross-section mould is obviously more difficult to demould rather than a draft angled mould because of excessive adhesion and friction: the rectangular profile has a tendency to lock against plastic features. However, the challenges remain on how to generate controlled draft angles and fillet radii. Conventionally, micro milling [26], lithography and electroforming [27, 28], and additive manufacturing [29, 30] commonly used microfabrication techniques in manufacturing microscale surface structures on micro mould tool inserts. Considering a microfluidic chip as an illustrative example: a channel feature generally ranges between tens of microns to several hundred microns in both width and depth [31–33]. For most applications, the corresponding mould tools are required to have high surface structure integrity, a mirror-like finish with low surface roughness (<50 nm) [34], and a possible draft angle to ease the demoulding of plastics from the mould. However, depending on the feature sides, it is quite challenging to control the draft angle of micro scale structures of the mould based on conventional micro milling or micro electroforming for features smaller than 100 μm. For micro milling, this is due to large cutting tool diameters and precision positioning accuracy requirements for the machine tools; for micro electroforming, it is determined by the master created by deep reactive ion etching or UV lithography, where the draft angle is difficult to control because of the way in which UV lithography exposure creates straight profiles. For additive manufacturing of micro-structured mould tools, the precision remains too low at present to be a viable production route for moulds for micro injection moulding.

Based on this challenge, we propose to use a non-contact electrochemical polishing method to shape/round the walls, edges and corners of micro mould tools. Electropolishing (EP) is a non-contact machining process that cleans [35], passivates [36], deburs [37] and forms [25] the metal surface. The resulting metal is shiny and free of surface defects. It has diverse manufacturing applications including μ-MEMs [38], μ-optics [39] and μ-TEM [40] samples. Principally, it is based on Faraday's law which states that the material removal rate is directly related to the supplied current. It consists of a cell where the anode (work piece) and cathode (counter electrode) are immersed in an electrolyte; anodic dissolution of metal occurs based on a current density gradient; and it can lead to the controlled forming and shaping of micro features. The current density gradient is uneven, and higher at protrusions than at recessed regions [41]. This leads to localised material removal. The principal of EP can be used to shape/round the geometric features of mould tools whereby more material is removed from the micro walls and edges than the base. Such a geometric change, i.e., increase
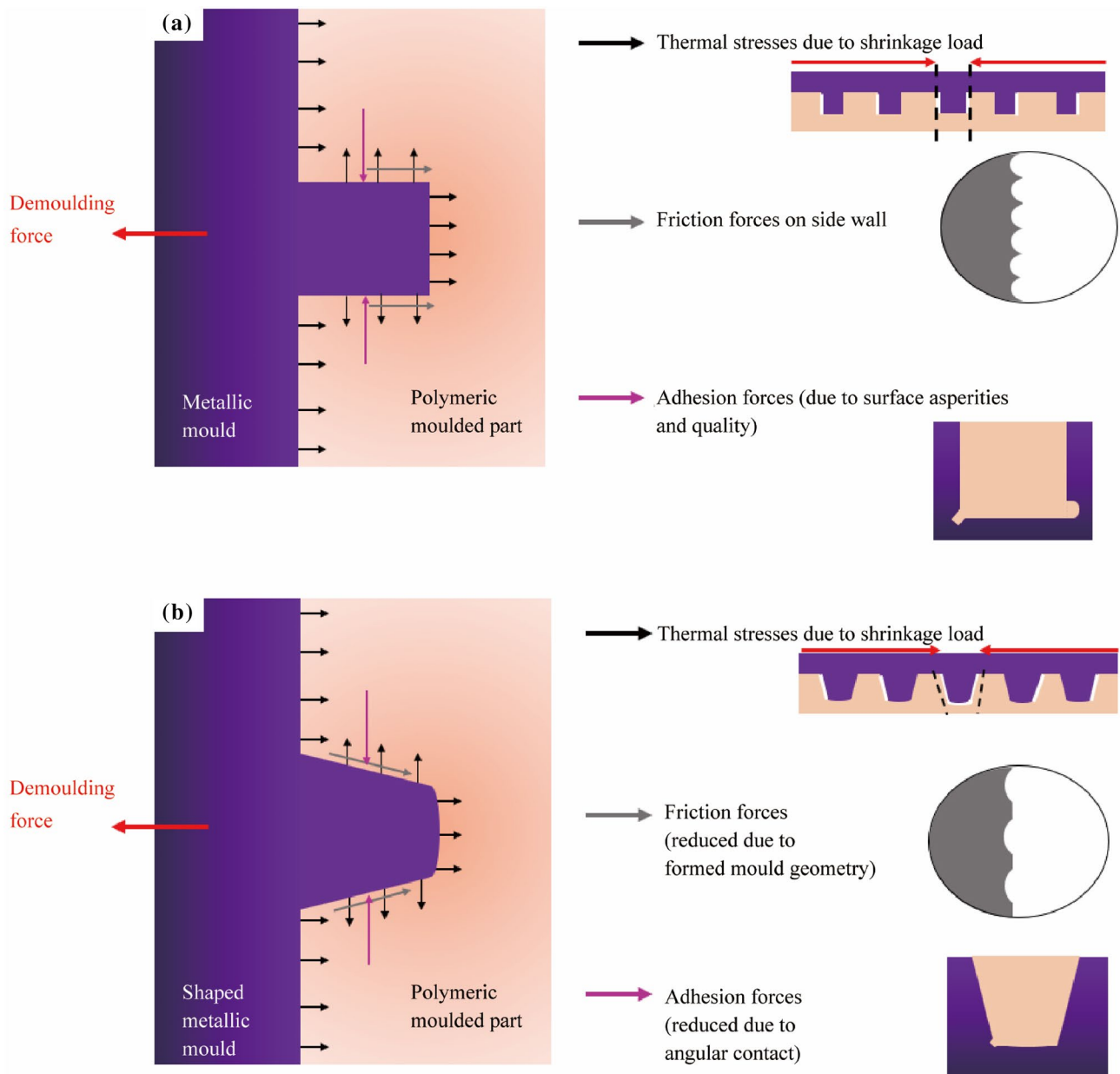
Fig. 1 Schematic of demoulding forces showing the interaction between metallic mould and replicated polymeric part when the microscale ridges either **a** linear (e.g., manufactured via UV LIGA and electroforming), or **b** shaped or formed in cross-sectional profile after non-contact electrochemical machining

in draft angle and fillet radius, can reduce the occurrence of demoulding defects without altering the effective operation of the designed component. Therefore, EP is a suitable technique to shape and round the micro features of mould tools where other microfabrication processes cannot be used.

In the present study, we aim to shape and round the micro-Ni mould fabricated through silicon dry etching, electro forming and moulding (DEEFM) with designed multi-linear ridges and star patterns. Due to the anisotropic nature of dry etching, it is not possible to form

a draft angle or to control any radius at the edge of a mould ridge. The developed multiple-linear ridges and star patterns range in dimensions from tens to hundreds of microns for a broad spectrum of microfluidic features and functional surfaces, that are nominally rectangular in cross-section. This present paper tests the hypothesis that EP can effectively shape and round such features (increase fillet radius and achieve a positive draft angle) and thus effect minor changes to surface morphology. Micro mould features are arranged in the form of linear
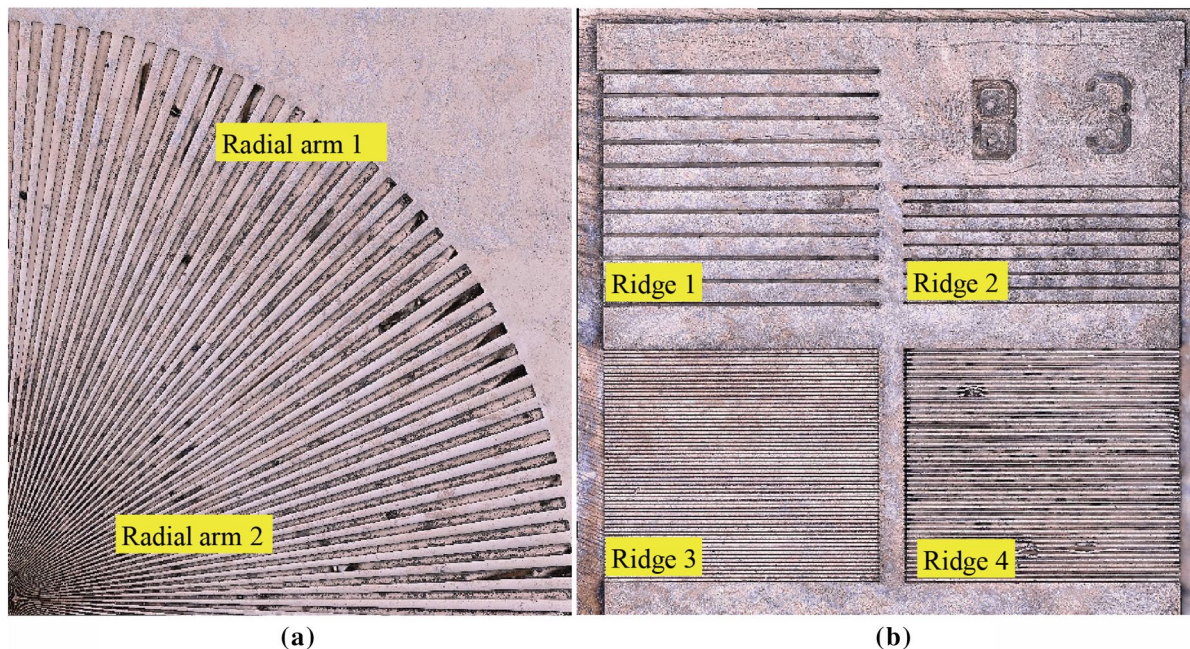
ridges and radiating star patterns, the dimensions of which range in width from 15 µm to 150 µm, gap distance from 10 µm to 130 µm and height from 80 µm to 100 µm. Most microfluidic devices have features with such common dimensions. An initial characterisation study (not shown) was conducted on micro mould Ni tools in various electrolytes ranging from strong to weak acids which showed the changes in feature topography, morphology and oxide layer deposition on the mould tools. That study showed that no oxide layer was deposited when using a nickel sulfamate solution and this electrolyte was selected for the present work and process parameters, i.e., voltage (V), time (min) and temperature (°C) were optimised to quantify shaping and surface roughness. Knowing that EP changes the shape and form of micro features according to the current density gradient of a feature, we have undertaken a detailed analysis to characterise and quantify the shaping and polishing effect on feature topography (i.e., draft angle and fillet radius) and surface morphology (surface roughness, S_a). Initially, the process of shaping and rounding brings a good geometric change that improves the mould design but surface morphology is a bit disturbed, i.e., S_a gets high. This issue will be addressed in future studies by combining the effects of shaping and polishing through use of pulsed currents. Such changes to the profile of a feature can significantly ease demoulding by reducing the friction and adhesion forces and thermal stresses associated with a particular microfeature.

2 Design methods and materials

2.1 Multi-linear and star patterns

The designed micro patterns on a pure Ni (99.5%) wafer took the form of multi-linear ridges and star shaped structures; these were manufactured using dry etching, electroforming, and moulding based on silicon lithography [42] and electroforming [43]. Two design structures were patterned on 4-inch silicon wafers using ultraviolet lithography, deep reactive ion etching (DRIE), followed by a conductive layer of titanium (50 nm) and nickel vanadium (200 nm), which was electroformed and then etched in a solution of potassium hydroxide (KOH). Feature dimensions of multi-linear ridges varied in width from 15 µm to 150 µm, gap distance from 10 µm to 50 µm and height from 80 µm to 100 µm, while star patterns had an outer diameter of 9 000 µm, inner core diameter of 80 µm, with radial arms of width from 10 µm to 150 µm, gap distance varying from 10 µm to 130 µm and height from 80 µm to 100 µm. Figure 2 shows the samples containing multi-linear and star patterns on a Ni wafer: the area containing the linear patterns was nominally 7.5 mm × 15 mm while that containing the star patterns was 6.8 mm × 14 mm.

Normally, microfluidic devices have such dimensions in most of their applications. This study is focused on the effects of precision shaping and rounding of Ni mould micro features after EP which will reduce the demoulding defects and improve replication efficiency. The detailed

Fig. 2 Ni mould having micro star patterns **a** two radial arms marked (radial arm 1 and radial arm 2), and **b** linear ridges (four ridges marked: 1, 2, 3 and 4)

dimensions of the linear ridges and star arms are given in Table 1.

2.2 EP setup

A DC current supply (Owon ODP3033, 5642JA Eindhoven, the Netherlands) with two power channels, having voltage and current at a maximum rating of 60 V and 3 A, was used for EP. The electrolyte solution was prepared with a 2 mol/L nickel sulfamate solution ($H_4N_2NiO_6S_2$, Ampere Galvanik Germany) with the addition of boric acid (20–30 g) and a wetting agent (1 mL). Ni mould tools with linear micro ridges and star patterns act as the anode and a flat SS cathode is used, both of which are connected to a DC power supply. There is anodic dissolution of Ni in the solution of nickel sulfamate and this leads to shaping and rounding of micro features. The electrochemical cell in Fig. 3, describes the geometric and morphological changes after EP.

2.3 Sample preparation

The designed micro patterns of star features and multi linear ridges were prepared with effective areas of 94.9 mm^2 and 110 mm^2. These samples were given an ultrasonic bath in deionized water (5 min) and acetone (5 min) to increase the surface reactivity. In order to insulate the unpolished surface, the back sides of the samples were coated with an aerosol conformal coating; the operating temperature of which remained between +200 °C and −70 °C.

2.4 Measurement of geometric changes after EP

The designed micro patterns of the star features and multi linear ridges were analysed before and after EP in order to examine any changes in topography and morphology. In order to quantify the geometric changes after EP in terms of draft angle and fillet radius, 2D profiles were observed for the multi-linear ridges and radial star arms. Four points were taken along the length of each ridge and arm to note variations in each for draft angle and fillet radii.

Table 1 Dimensions of Ni mould having star pattern and linear micro ridges

Micro features	Star patterns (sample 1 (S_1) and sample 2 (S_2))		Linear ridges (sample 3 (S_3) and sample 4 (S_4))			
	Radial arm 1	Radial arm 2	Ridge 1	Ridge 2	Ridge 3	Ridge 4
Width/μm	110	45	150	90	20	15
Height/μm	100	100	100	100	80	80
Gap distance/μm	130	80	50	40	10	20

Note: There are four samples, samples 1 and 2 (star patterns observed at two radial arms) and samples 3 and 4 (multi-linear ridges observed at four ridges).
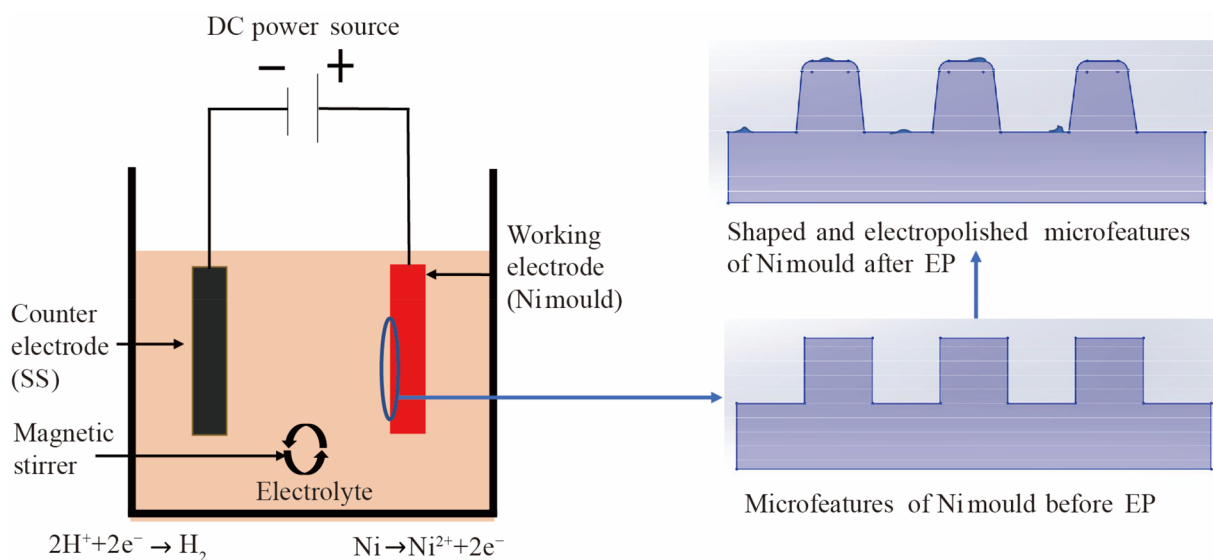
Fig. 3 Electropolishing cell for Ni mould showing changes in feature topography and surface morphology after EP

The measurements for draft angle were taken using Bruker software vision 64, which gave 2D profiles of features. Subsequently, the profile was exported and analysed in Matlab by extracting the corner radii of microfeatures before and after EP. A curve fitting technique was used to note the radii from both the left- and right-hand sides and an average was examined. The geometric changes in the microfeatures after EP, along with the measurement of draft angle and fillet radii are detailed in Fig. 4. All samples are analysed using a 3D profilometer before and after the EP process to capture the profiles.

2.5 Characterization of samples

A digital microscope (AmScope MU1000 with 10MP) was used to identify the characteristic dimensions on the two mould patterns. Star patterns were examined at two areas, the outer and inner radial arms, as shown in Fig. 5. Likewise, four ridges were observed on the multi-linear samples to quantify any variations in width and gap distance, as shown in Fig. 6. The surface morphology and topography of the features were evaluated using white light interferometry (NP Flex Bruker, USA) at $20\times$ magnification. The shape, depth and surface roughness of the features were quantified. A benchtop SEM TM-4000 using standard electron (SE) beams and back scattered electron (BSE) beams, with high accelerating voltages (5 kV, 15 kV and 20 kV) and magnifications ranging from $25\times$ to $250\,000\times$ was used to ascertain the shaping effects of electropolishing along the corners and edges of the micro features.

## 2.6 Characterization of nickel sulfamate electrolyte

Unlike other conventional acids, i.e., sulphuric and phosphoric acid, a green solution of nickel sulfamate has been selected. The solution of nickel sulfamate was characterized using a CS310 electrochemical work station (Wuhan CorrTest, China). A polarization study was conducted in a three-electrode standard cell, where the Ni sample was used as an anode, 314 SS as the cathode and Ag/AgCl as a reference electrode using linear scanning voltammetry (LSV) with a positive sweeping potential of $6-0$ V at a scanning speed of 10 mV/s. Previous studies examined the potentiodynamic polarization behaviour of Ni in a nickel sulfamate solution to observe changes in shaping and polishing at different voltages [44]. The polarization study identified regions of etching, polishing, and gas evolution, as depicted in Fig. 7.

2.7 Numerical simulations for electrochemical polishing

A 2D transient analysis was undertaken using COMSOL Multiphysics 5.4 on Ni microfeatures to predict the pattern of current density distribution on the four linear ridges in order to better understand geometric changes that occur during electropolishing. Two equations of state were used, i.e., deformed geometry (DG) and electric currents (EC) with a time dependent solver. Geometry deformation is a function of normal current density on the surface [45]
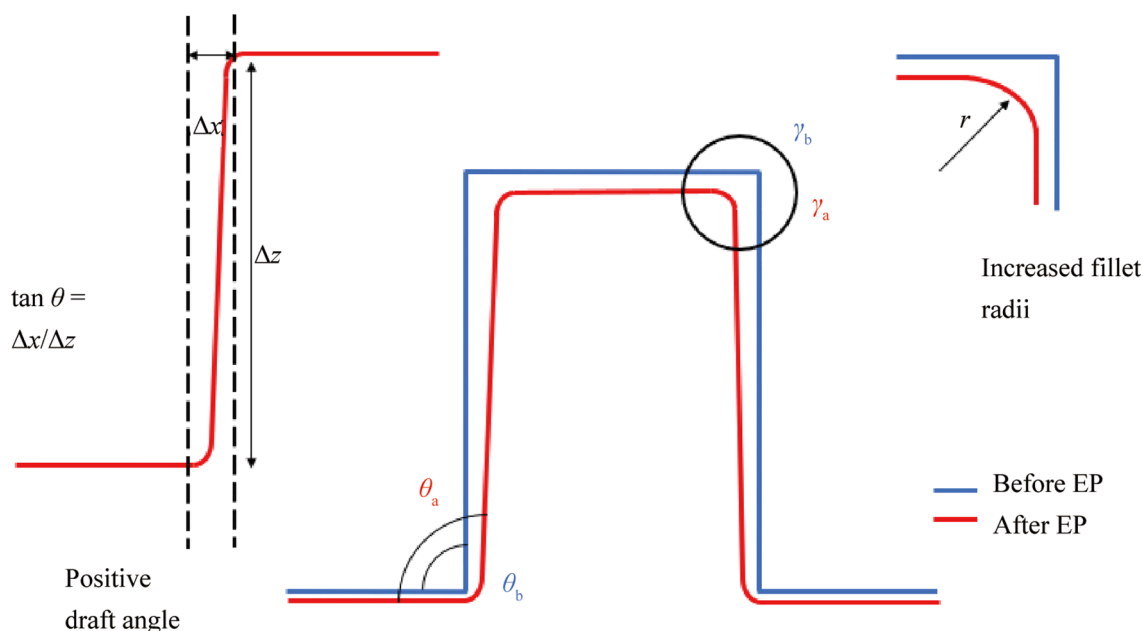
Fig. 4 Micro features being shown with the geometric changes which occur after EP, the measurements for draft angle and fillet radii being indicated
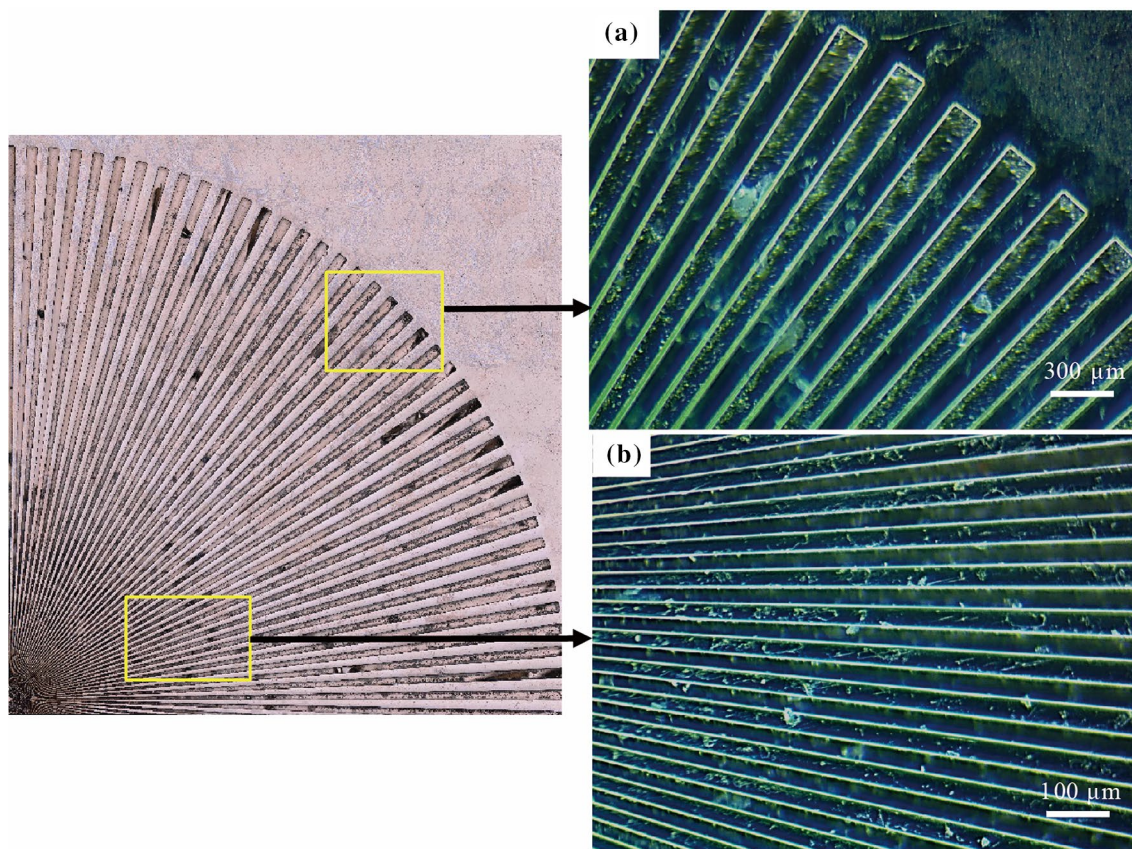
Fig. 5 Ni mould with star patterns were observed using optical microscope **a** outer radial arm S_1 with width= 110 µm and gap=130 µm, and **b** inner radial arm S_2 with width= 45 µm and gap= 80 µm

$$V_{\text{def}} = -kJ_{\text{n}}, \tag{1}$$

where V_{def} is the normal mesh velocity/ deformation, k a proportionality constant (based on surface normal vector and specific removal volume), and J_{n} current density

$$J_{\text{n}} = \sigma E. \tag{2}$$

Furthermore, current density J_{n} is dependent on the electrical conductivity σ and electric field E.

The initial boundary conditions for defining anode, cathode, normal velocity for deformation and initial potential are shown in Fig. 8. The time dependent response is governed by electric charges, material relativity and voltage gradient

$$\nabla J = Q_{jv}, \tag{3}$$

$$J = \sigma E + \frac{\partial D}{\partial t} + J_{\text{e}}, \tag{4}$$

$$E = -\nabla V, \tag{5}$$

where D is a relative permittivity term which is based on ε_{o}, the absolute permittivity and ε_{r}, the relative permittivity

of the materials. Q_{jv} the change rate of electric charge per unit volume, and J_e the current density of external electric current.

The 2D model of the Ni micro mould employs a variable triangular mesh density. A finer mesh was applied overall to simulate geometric deformations after electropolishing. In addition, an extremely fine mesh with higher density was used near the anode region to capture critical areas accurately.

The model is simplified by a few assumptions about the boundary conditions and equations of state (EC and DG), namely:

(i) Anode boundary constitutes the micro feature, cathode boundary is a flat surface and electrolyte sets positive voltage at anode and grounds the cathode.
(ii) Current distribution is governed by Ohm's law with uniform electric field and is based on a time dependent solver.
(iii) Geometric deformations are based on Laplace mesh smoothing of the 2nd geometric order.
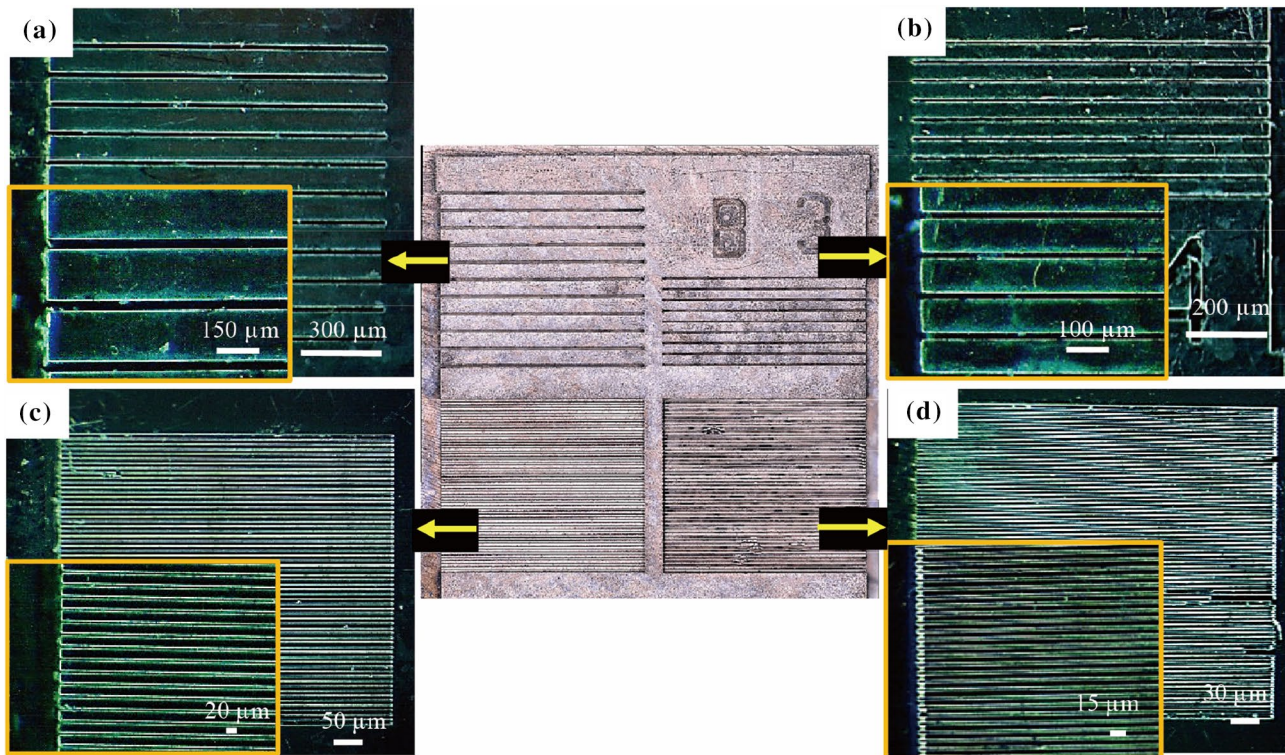
Fig. 6 Ni mould with multi-linear ridges being observed using optical microscope **a** ridge 1 with width=150 μm and gap=50 μm, **b** ridge 2 with width=90 μm and gap=40 μm, **c** ridge 3 with width=20 μm and gap=10 μm, **d** ridge 4 with width=15 μm and gap=20 μm
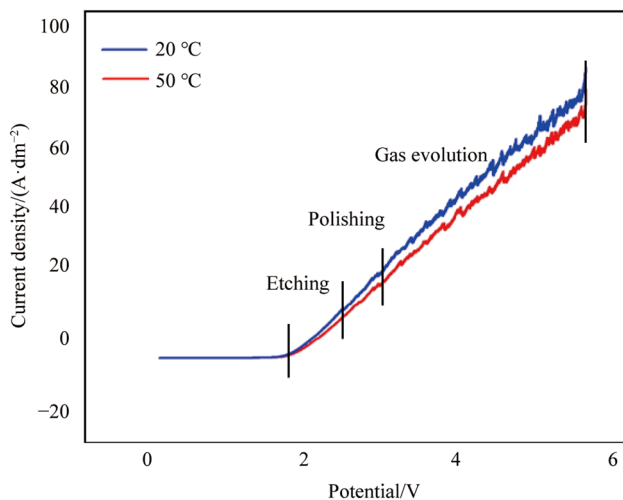
Fig. 7 Polarization curve of Ni mould in the solution of nickel sulfamate

This model validates the principal of EP as it confirms the uneven current distribution pattern and geometric change leading to shaping and forming of the micro features.

3 Results and discussion

3.1 EP and shaping of multi-linear ridges and star patterns

The various linear micro ridges and star patterns were electropolished in the nickel sulfamate solution. The characterization of electrolyte in Fig. 7 shows the regions of etching, polishing and gas evolution. It has been observed that the region of etching has no effect on shaping and rounding of Ni micro features while the gas evolution will lead to pitting and passivation of Ni mould, and only the polishing region from 2.8 V to 3.0 V shapes and rounds the Ni mould with a positive change in draft angle and fillet radii. Previous work by the present authors characterised the use of EP on shaping and polishing the micro features of a mould tool using various electrolytes (from strong to weak acids). Based on the optimal results of that work, the EP parameters of voltage, temperature, agitation and electrode gap were fixed in this present study.

Time was varied, however, in order to observe changes in feature topography and the surface morphology of microfeatures. The process parameters are summarised in Table 2.

EP of Ni micro moulds in the solution of nickel sulfamate proved effective in shaping and polishing of the multi-linear
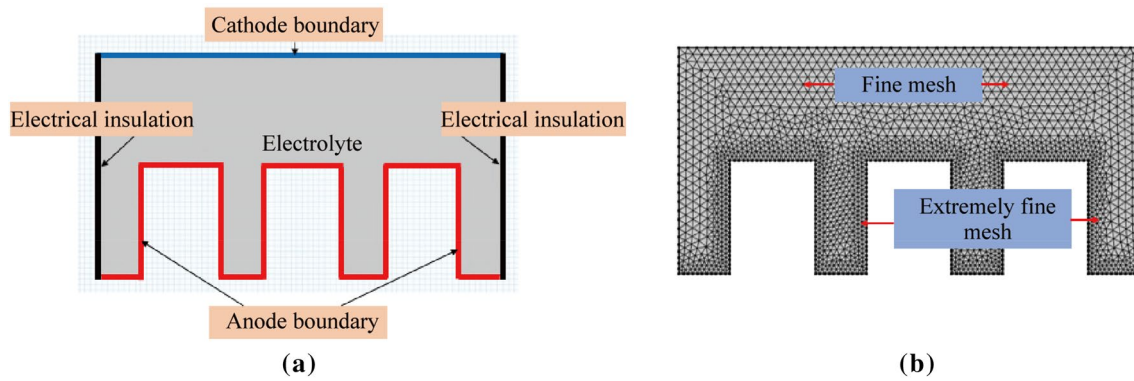
Fig. 8 2D model of Ni mould with microridges indicating **a** initial boundary conditions, and **b** variable mesh densities

Table 2 Electropolishing parameters used for optimizing the shaping effect and surface roughness

Parameters	Star patterns		Linear ridge patterns	
	S_1	S_2	S_3	S_4
Voltage/V	3	3	3	3
Temperature/ºC	50	50	50	50
EP time/min	8	15	8	15
Area/mm^2	94.9	94.9	110	110
Current/A	0.097	0.100	0.129	0.128
Current density/(A · dm^{-2})	10.22	10.54	11.73	11.64

ridges and star pattern features. It was observed that when EP conditions of voltage (3 V), electrode distance (20 mm), temperature (50 °C) and magnetic agitation (200 r/min) were used; a change in time from 8 min to 15 min resulted in changes to the geometric features and surface roughness. These changes in surface morphology and feature topography are discussed below in Sects. 3.3 and 3.4.

3.2 Descriptive analysis of multi-linear ridges and star patterns

Following EP of the Ni micro features, i.e., multi-linear ridges and star patterns, changes to their shape and form have been characterised qualitatively by observing the geometric changes at the corners and edges of the microfeatures. Accompanying this, there was also a change in surface morphology, as measured by surface roughness (S_a). The micro features became more rounded and formed along the edges and corners after EP, as shown in the 2D Bruker images in Figs. 9 and 10. Besides the geometric change, there were also some bubbles and pitting marks on the samples, which represented a significant change in surface roughness, as evident in Fig. 9. Both star arms (radial arms 1 and 2) and linear

ridges (ridges 1–4) were examined to record the changes in feature topography and surface morphology.

3.3 Quantitative analysis of multi-linear ridges and star patterns

A detailed analysis has been performed to quantify the geometric changes in the micro features of both the multi-linear and star patterns. EP leads to localized material removal based on current density thus changing the draft angle and fillet radius of microfeatures. The 2D overlays of micro linear ridges and star patterns shows the thinning and shaping of features after EP in Figs. 11 and 12. The areas of higher current density are marked in Fig. 11 and material removal and shaping are most pronounced here. For each feature, the change in draft or taper angle and fillet radius was quantified by analysing the Bruker profilometry images. Geometric integrity was ensured by using the filters of statistic, data restore, remove tilt and Gaussian with long wave lengths of 0.01, 0.03 and 0.05 mm based on feature size to distinguish geometry and roughness. Furthermore, four points were taken on each micro ridge and star pattern to observe the change in draft angle and fillet radius.

Topographic changes to the nickel micro features are summarised in Tables 3 and 4 (each value is an average taken at four points along the ridge or radial arm). By increasing EP times, there is a change in geometry and more extensive forming is observed to occur, which is manifest in the form of increased fillet radius and positive draft angle. However, surface roughness also increases when the polishing time is increased from 8 min to 15 min. The samples of star patterns which are electropolished for 8 min (S_1-1 and S_1-2) have fillet radii of up to +3.58 µm, a positive draft angle of 2.16º–2.86º and an increase in surface roughness from 67.3 nm to 113 nm. For those polished for 15 min (S_2-1 and S_2-2), the fillet radii increase from +3.76 µm to 4.73 µm while a positive draft angle of up to 3.62º and an increased surface roughness from 53 nm to 410 nm was also noted.
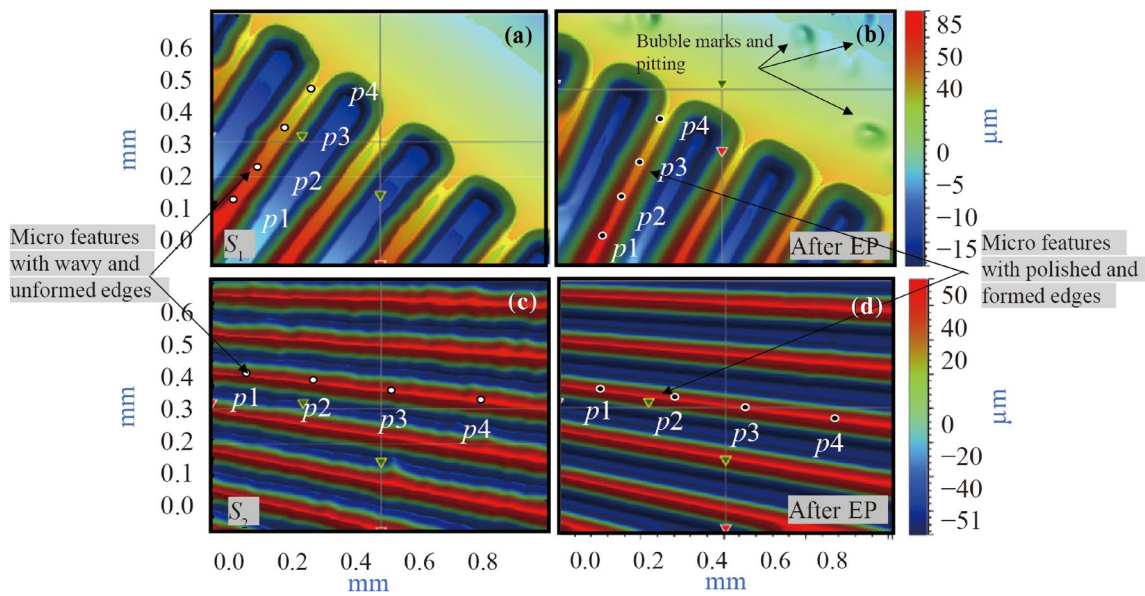
Fig. 9 3D images of Ni mould star patterns observed from the top; surface topography examined before and after EP **a**, **b** w=110 μm and h=100 μm (radial arm 1), **c**, **d** w=45 μm and h=100 μm (radial arm 2) (Four points are marked on the radial arms to record geometric changes after EP)

For the multi-linear ridges that were electropolished for 8 min (sample 3, ridges 1–4) the increase in the fillet radius ranges from +2.45 μm to 3.70 μm, while the draft angle increased by between 1.63° and 2.18°, and the surface roughness increased from 20.3 nm to 31.4 nm. For the ridge features that were polished for 15 min (4-1, 4-2, 4-3 and 4-4), the fillet radii increased by between 3.41 μm and 5.09 μm; a positive draft angle of between 2.1° and 3.58° was formed; and the surface roughness changed from 25.9 nm to 47.3 nm.

For both kind of patterns, the EP time adversely affects the quality of the surface roughness (S_a). Specifically, the surfaces developed pits and bubble marks on both the linear channel and star pattern samples.

Quantitative analysis of the star patterns has been performed by taking two points on each star sample (S_1-1 (point 1 on the outer edge of star pattern 1) and S_1-2 (the central region of star pattern 1) as indicated in Fig. 2). S_1 is the star sample which was electropolished for 8 min at 3 V and 50 ℃ while S_2 is the star sample electropolished for 15 min using the same parameters. The changes in fillet radius and draft angle have been recorded at four points along a radial arm of each star pattern and average values are shown in Table 3. Likewise, four multi-linear ridges with widths ranging from 15 μm to 150 μm, heights from 80 μm to 100 μm and gaps from 10 μm to 130 μm on samples 3 and 4 were analysed, the results of which are summarised in Table 4. Sample 3 was electropolished for 8 min at 3 V and 50 ℃ while Sample 4 was the multi-linear sample that was electropolished for 15 min using the same parameters. For each of the multi-linear ridge samples, the changes in draft angle and fillet radii were noted at four points along the width of ridges and average values with standard deviations are indicated in Table 4. Overall, after selective polishing, the draft angle of the micro patterns increased by 1.63°–3.58°, while the fillet radii of the features increased by 5.09 μm. Although the surface roughness of the mould also increased, it still remained below 50 nm, which was sufficiently good to mould optically transparent products [34].

3.4 SEM analysis

Two phenomena are associated with EP: one is the precise geometric change in the topological shape of the micro features, and the other is the change in surface roughness. Additional insights into the phenomenon of shaping and rounding of the edges and corners of the linear micro ridges and star patterns were obtained by means of SEM inspection. The surface morphology and topography can be seen in Figs. 13–16. As the EP time increaseed from 8 min to 15 min, more significant rounding was observed around the corners and edges of star patterns while the surface roughness increased. There were some marks observed on the star patterns (see Fig. 13) after EP in the solution of nickel sulfamate for 8 min while pitting was observed on the star patterns (see Fig. 14) that were electropolished for 15 min.

Likewise, the SEM analysis for the multi-linear patterns highlights the topographical and morphological changes clearly in Figs. 15 and 16. Ridges 1–4 were imaged to observe the side walls and surface roughness. The phenomenon of rounding and shaping can be seen in the SEM images
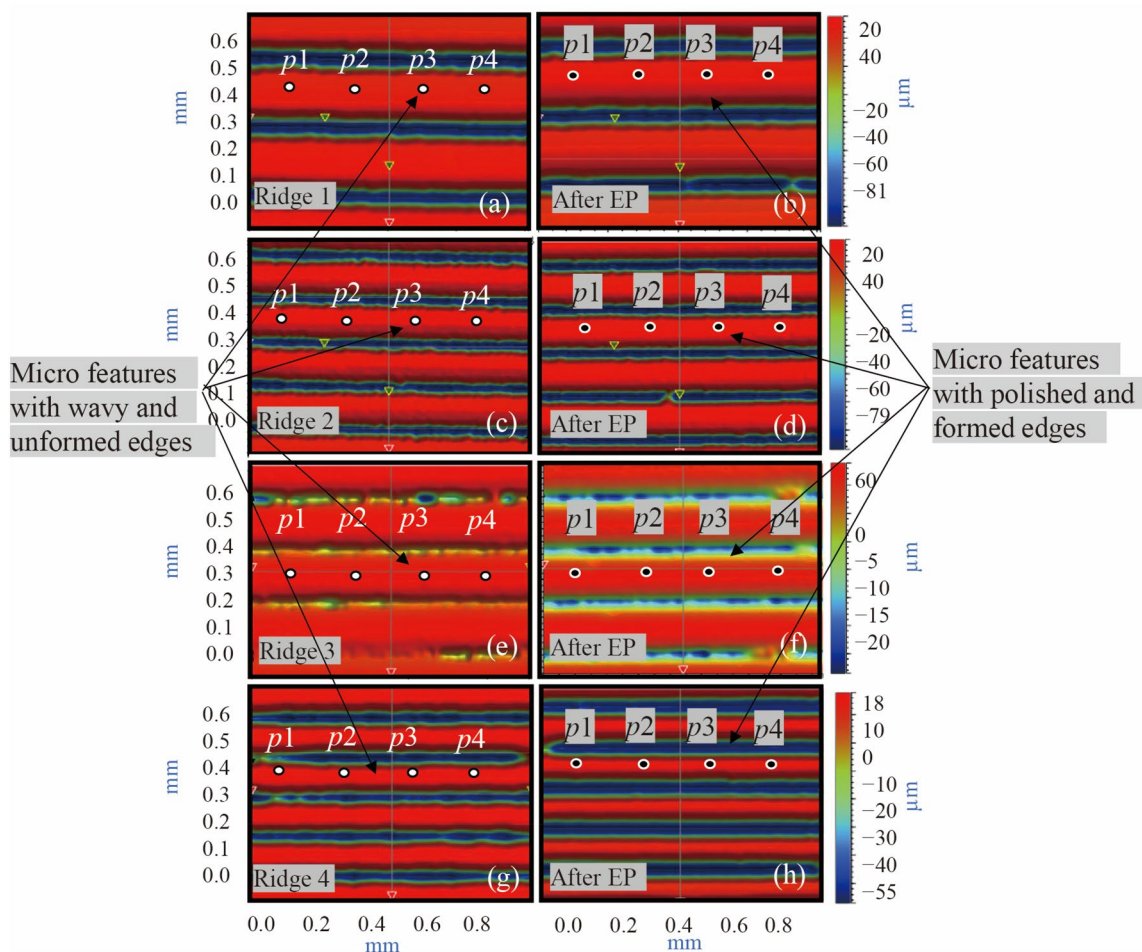
Fig. 10 3D images of Ni multi-linear patterns observed from the top, surface topography examined before and after electropolishing for four ridges **a**, **b** $w=150$ μm and $h=100$ μm, **c**, **d** $w=90$ μm and $h=100$ μm, **e**, **f** $w=20$ μm and $h=80$ μm, **g**, **h** $w=15$ μm and $h=80$ μm (Four points are marked on the linear ridges to record geometric changes after EP)

of the samples before and after EP. Increasing the EP time results in more material removal and provides more prominent shaping effects but also increases the surface roughness. Depending on the application that might be intended for such features, further optimization of EP parameters could serve to combine the shaping and polishing effects together.

3.5 Numerical simulations of shaping and rounding of microscale features

EP has the potential to shape and round microscale features of Ni principally as the current density distribution is higher at the corner and edges in comparison to the base region. This results in more material removal at the corners and edges, resulting in shaping and rounding of microfeatures. In our experimental analysis, it can be seen clearly that EP changes the feature topography by increasing the draft angle and fillet radius. This change is also reflected in our numerical simulations which modelled the EP of linear micro ridges

of Ni with varying width, height and inter gap spacing (electrical currents and geometric deformation to highlight the material removal process).

Numerical simulations have been performed on the linear micro ridges to observe the pattern of current density distribution and geometric deformations after EP. Figure 17 shows the electropolished micro ridges with dimensions of width ranging from 15 μm to 150 μm, height from 80 μm to 100 μm and gap width ranging from 10 μm to 50 μm. The four linear ridges having different dimensions and aspect ratios show EP results. It is observed clearly that all microridges have a higher current density at the corners, which confirms the physical reality of EP whereby greater amounts of material removal occurs for the micro features along their edges and corners, thus resulting in changes to the draft angle and fillet radii. As the feature size and aspect ratio changes, the effect also changes and is most significant for ridge 4, which has a width of 15 μm, height of 80 μm and inter gap
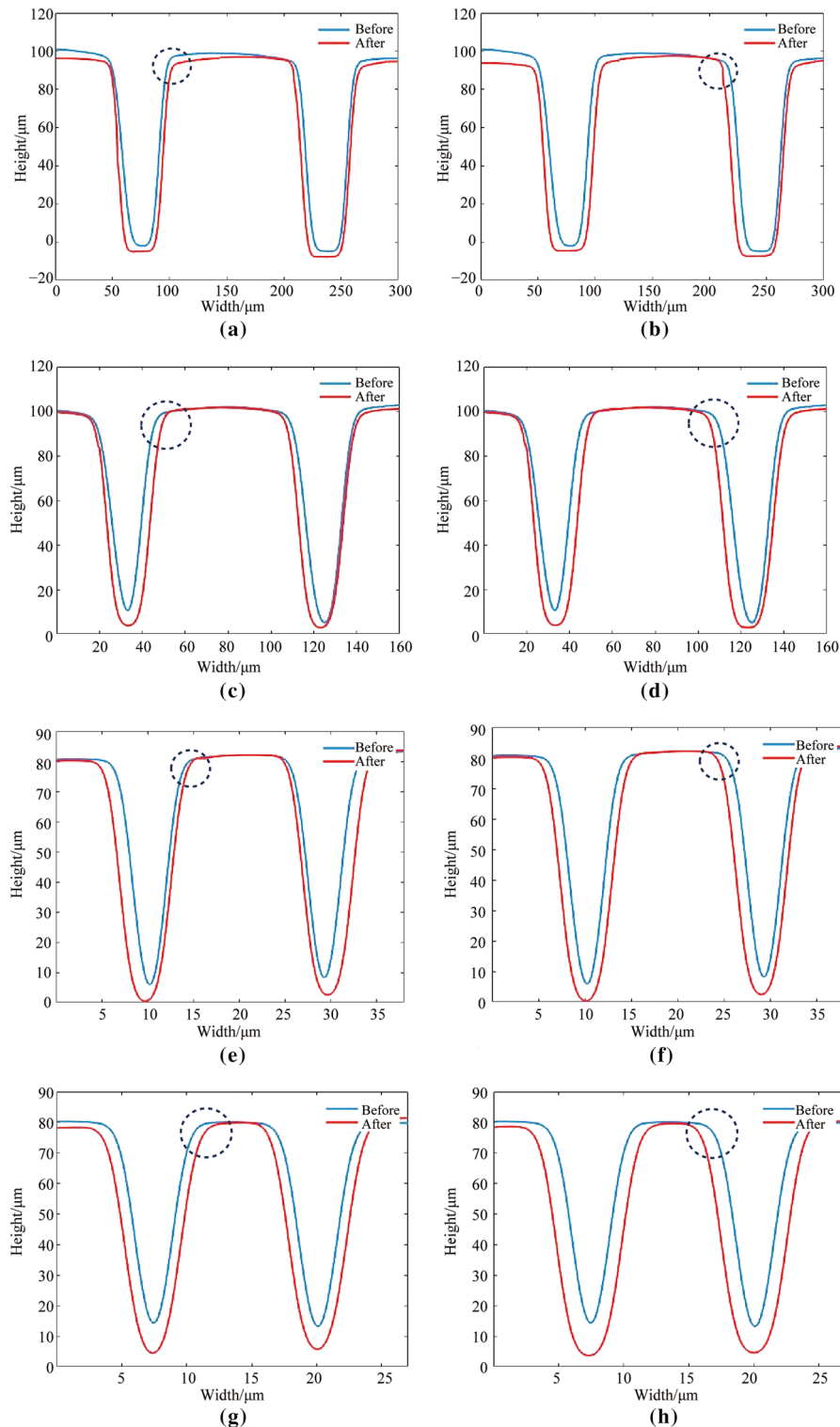
Fig. 11 2D overlays of Ni multi-linear ridges showing the geometric change in profile (increase in fillet radii and positive draft angle) after EP for 8 min and 15 min **a**, **b** ridge 1: $w=150$ μm, $h=100$ μm, **c**, **d** ridge 2: $w=90$ μm, $h=100$ μm, **e**, **f** ridge 3: $w=20$ μm, $h=80$ μm, **g**, **h** ridge 4: $w=15$ μm, $h=80$ μm (The areas of higher current density are marked which leads to more material removal and shaping phenomenon)

spacing of 20 μm. The current density pattern is indicated in experiments (see Fig. 11) and simulations (see Fig. 17) of micro linear ridges, and is more intense at the corners.

Thus the numerical simulation validates the current density distribution and predicts the pattern of shaping and rounding after EP.
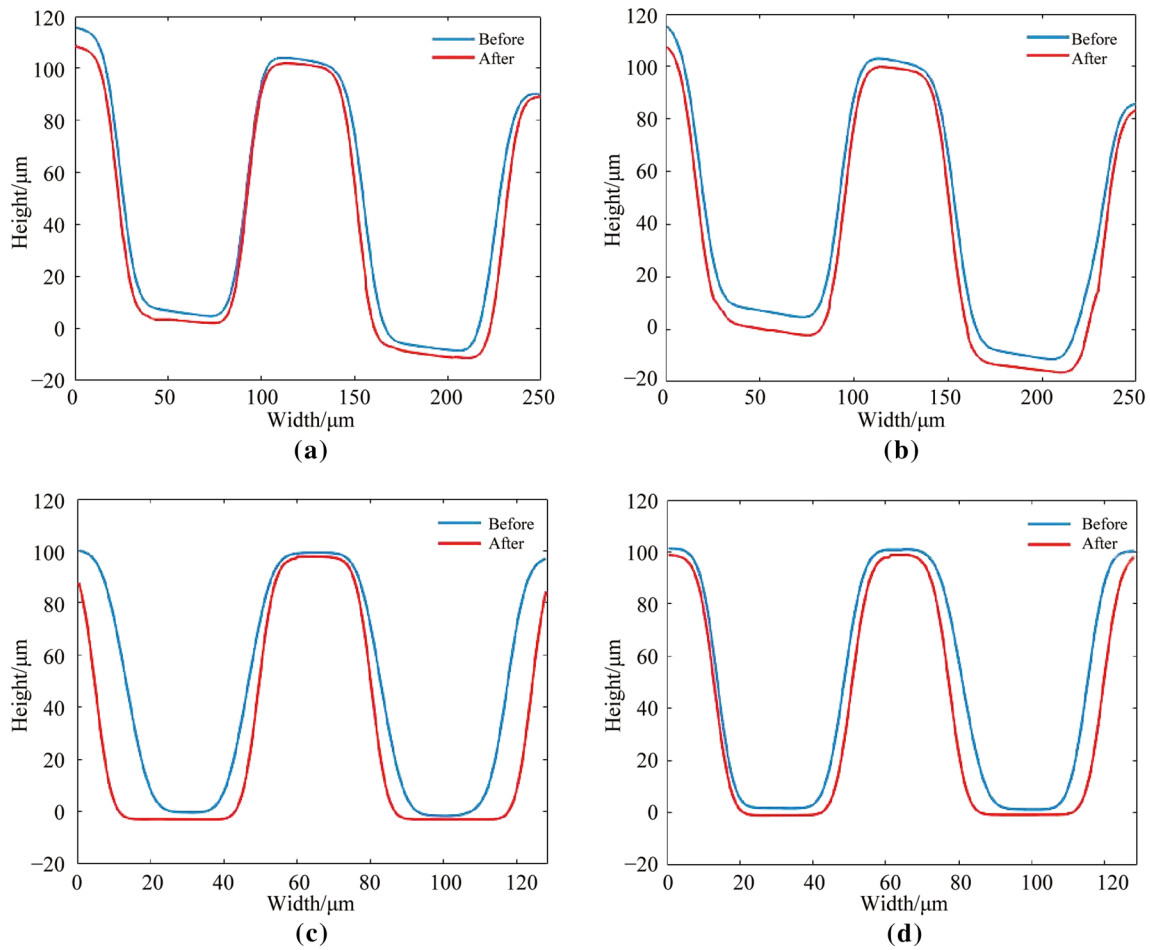
Fig. 12 2D overlays of Ni star patterns showing the geometric change in profile (increase in fillet radii and positive draft angle) after EP for 8 min and 15 min **a**, **b** radial arm S_1: $w = 110$ μm, $h = 100$ μm, **c**, **d** radial arm S_2: $w = 45$ μm, $h = 100$ μm

Table 3 Electropolishing results for star patterns in the form of shaping and change in surface roughness (Star patterns shaped and EP in nickel sulfamate solution)

| Sample	Dimension/μm	Positive change in draft angle/(°)	Increase in fillet radius / μm	Surface roughness (S_a)/nm		Remarks
				Before	After	
S_1-1	$w = 110$, $h = 100$	2.16 ± 0.56	3.58 ± 0.99	67.3	113	Fillet radius increases by 3.58 μm, and draft angle increases by 2.16°, and S_a increases from 67.3 nm to 113 nm.
S_1-2	$w = 45$, $h = 100$	2.86 ± 0.61	3.50 ± 0.33			Fillet radius increases by 3.5 μm, and draft angle increases by 2.86°, and S_a increases from 67.3 nm to 113 nm.
S_2-1	$w = 110$, $h = 100$	3.56 ± 0.82	4.73 ± 0.72	53	410	Fillet radius increases by 4.73 μm, and draft angle increases by 3.56°, and S_a increases from 53 nm to 410 nm.
S_2-2	$w = 45$, $h = 100$	3.62 ± 0.29	3.76 ± 0.38			Fillet radius increases by 3.76 μm, and draft angle increases by 3.62 °, and S_a increases from 53 nm to 410 nm.

Note: All linear dimensions in μm and angles in degrees (width "w", and height "h"), S_1-1 (star sample 1-radial arm 1) and likewise.

Table 4 Electropolishing results for multi-linear patterns in the form of shaping and change in surface roughness (Multi linear micro ridges electropolished in nickel sulfamate solution)

Sample	Dimension/μm	Positive change in draft angle /(°)	Increase in fillet radius /μm	Surface roughness (S_a)/nm		Remarks
				Before	After	
S_3-1	$w = 150$, $h = 100$	2.18±0.62	3.70±0.59	20.3	31.4	Fillet radius increases by 3.7 μm, and draft angle increases by 2.18°, and S_a increases from 20.3 nm to 31.4 nm.
S_3-2	$w = 90$, $h = 100$	1.94±0.44	3.54±0.61			Fillet radius increases by 3.54 μm, and draft angle increases by 1.94°, and S_a increases from 20.3 nm to 31.4 nm.
S_3-3	$w = 20$, $h = 80$	1.84±0.20	2.45±0.28			Fillet radius increases by 2.45 μm, and draft angle increases by 1.84°, and S_a increases from 20.3 nm to 31.4 nm.
S_3-4	$w = 15$, $h = 80$	1.63±0.27	2.58±0.33			Fillet radius increases by 2.58 μm, and draft angle increases by 1.63°, and S_a increases from 20.3 nm to 31.4 nm.
S_4-1	$w = 150$, $h = 100$	3.54±0.54	5.09±0.10	25.9	47.3	Fillet radius increases by 5.09 μm, and draft angle increases by 3.54°, and S_a increases from 25.9 nm to 47.3 nm.
S_4-2	$w = 90$, $h = 100$	3.58±0.60	4.89±0.67			Fillet radius increases by 4.89 μm, and draft angle increases by 3.58°, and S_a increases from 25.9 nm to 47.3 nm.
S_4-3	$w = 20$, $h = 80$	2.60±0.28	3.41±0.61			Fillet radius increases by 3.41 μm, and draft angle increases by 2.6°, and S_a increases from 25.9 nm to 47.3 nm.
S_4-4	$w = 15$, $h = 80$	2.19±0.32	3.43±0.42			Fillet radius increases by 3.43 μm, and draft angle increases by 2.19°, and S_a increases from 25.9 nm to 47.3 nm.

Note: All linear dimensions in μm and angles in degrees (width "w", and height "h"), S_3-1 (Linear sample 3- ridge 1) and likewise.
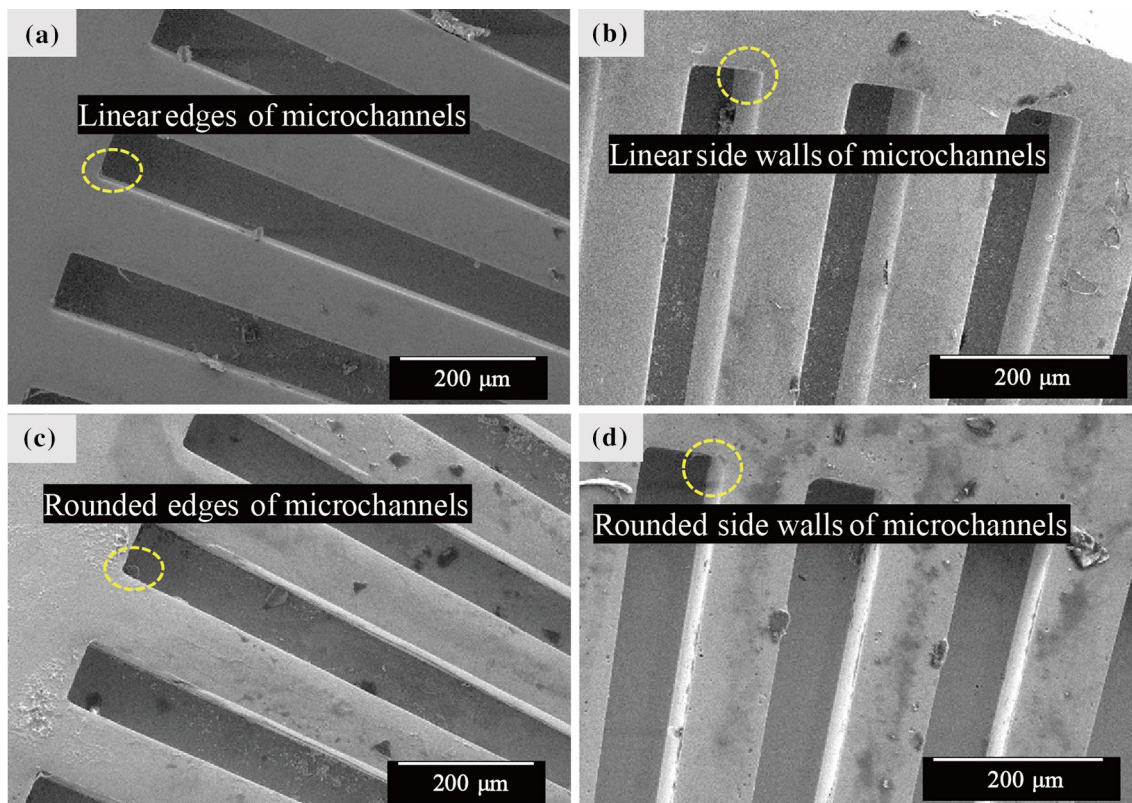
Fig. 13 SEM analysis for star pattern 1 **a**, **b** before EP, and **c**, **d** after EP for 8 min
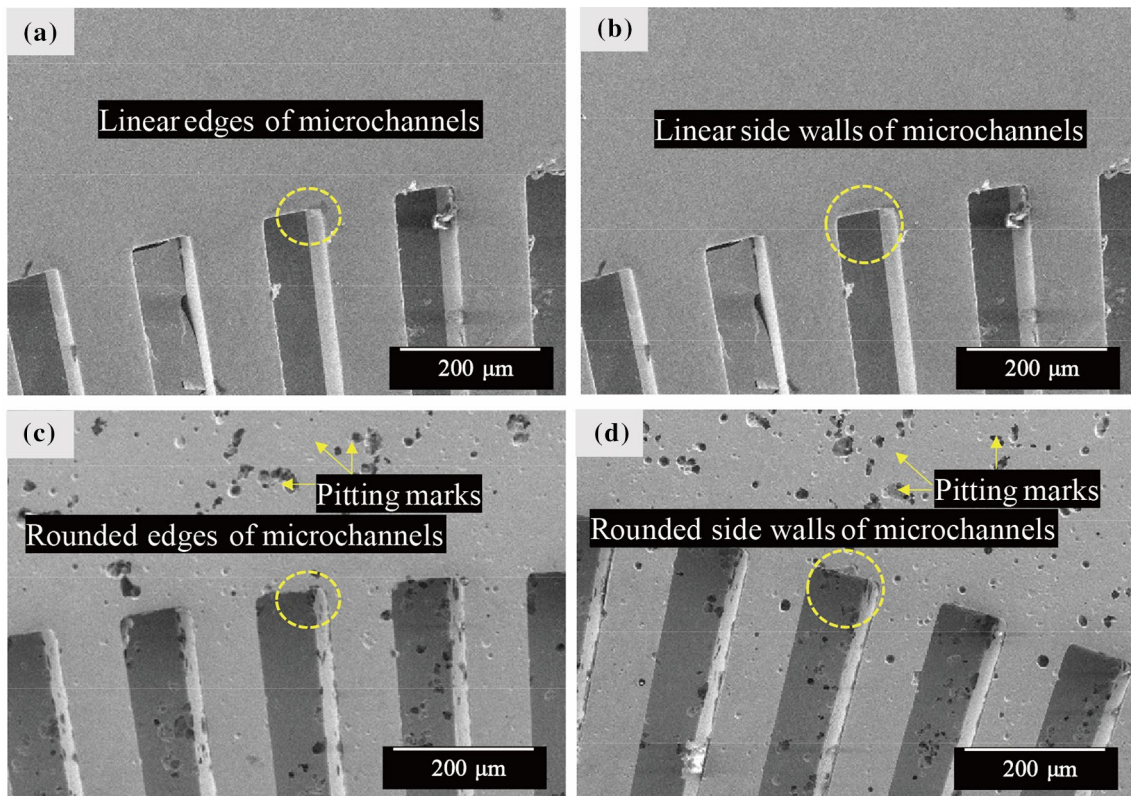
Fig. 14 SEM analysis for star pattern 2 **a**, **b** before EP, and **c**, **d** after EP for 15 min

4 Conclusions

The present study was conducted to optimize EP parameters when used for different micro mould patterns on a Ni surface, i.e., a star pattern and multi-linear ridges using a green solution of nickel sulfamate. EP is a non-contact electrochemical machining process that removes material based on the distribution of current density from the edges and corners of the microfeatures, thus resulting in the change of feature topography (i.e., draft angle and fillet radii) and surface morphology. Such geometric changes effected to mould tool inserts could help to ease demoulding and avoid the occurrence of defects caused by interfacial friction, adhesion and thermal stresses, and thereby improve the overall efficiency of a micro-injection moulding process. Subsequent experimental work will seek to examine this fully by comparing the ejection forces associated with electropolished and normal mould tool inserts, and to examine the associated defect rates. Optimized parameters for EP were based on our previous studies [19] to electropolish linear microfeatures of Ni in various electrolytes from strong to weak acids. A green solution of nickel sulfamate was thus selected to record the effects of shaping and rounding on star patterns and multi-linear ridges with dimensions ranging in width from 15 μm to 150 μm, gap distance from 10 μm to 130 μm and height from 80 μm to 100 μm by varying the EP time between 8 min and 15 min. The main conclusions are as follows.

(i)   Material removal rates by means of EP is proportional to the distribution of current density, which is higher at peak regions than at valley regions. When EP ridge and channel features on Ni micro mould tools, shaping of the features occurs in the form of an increase in the draft angle and fillet radii, and an increase in surface roughness. Optimized parameters for EP (voltage=3 V, temperature= 50 ℃, magnetic agitation= 250 r/min) were used to electropolish micro patterns in the form of multi-linear ridges and star patterns on a Ni surface. Using a nickel sulfamate solution and changing the polishing times from 8 min to 15 min, it was possible to characterise and quantify the resulting changes to the shape and roughness of the features. There were obvious changes around the edges and corners of the features while defects in the form of bubbles and pit marks were evident on the samples electropolished for the longer times (15 min; star 2 and sample 4). Bubble formation is linked to the generation of hydrogen gas at the cathode, resulting in continuous bubble formation and explosion during the EP process. The occurrence becomes more prominent
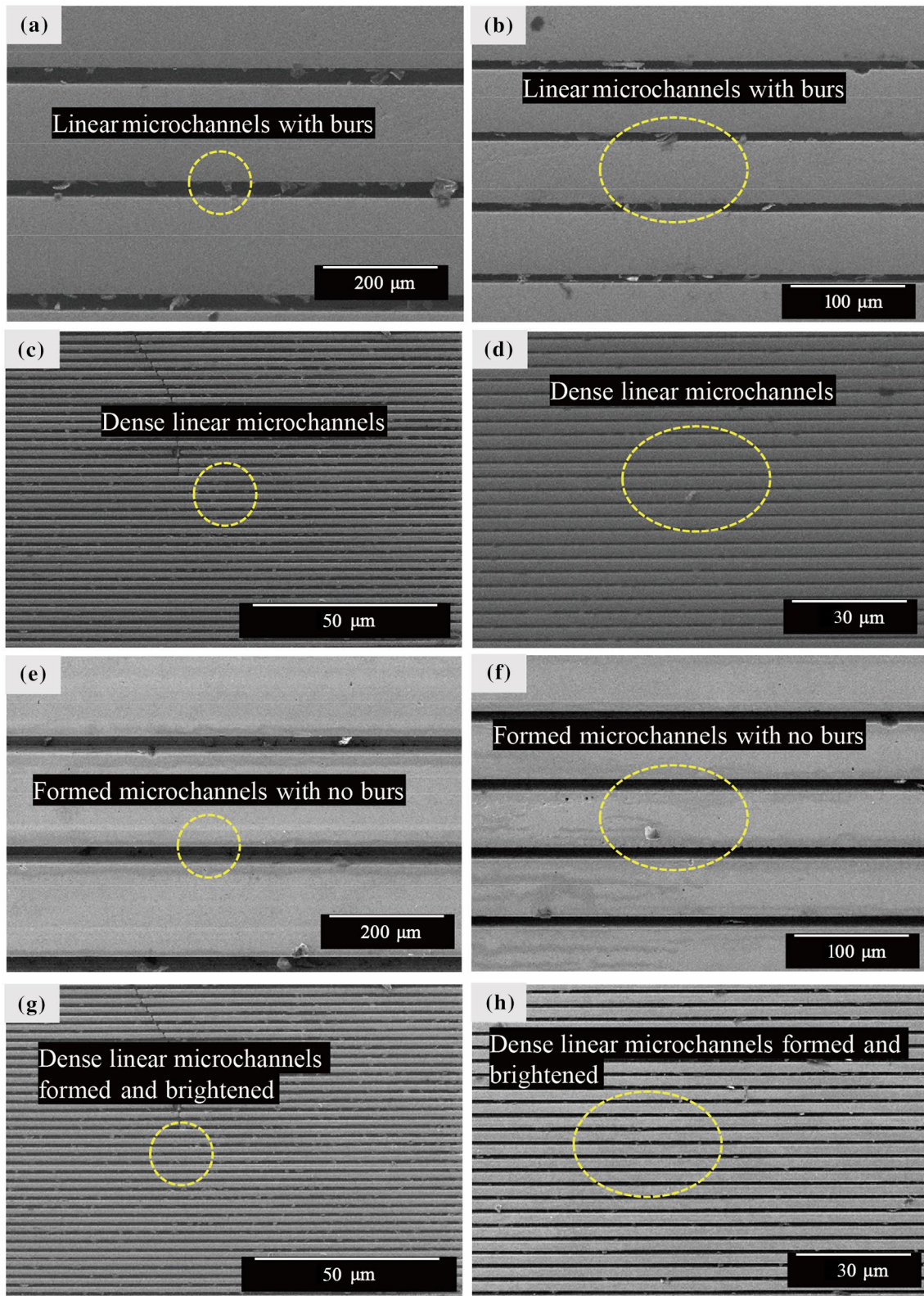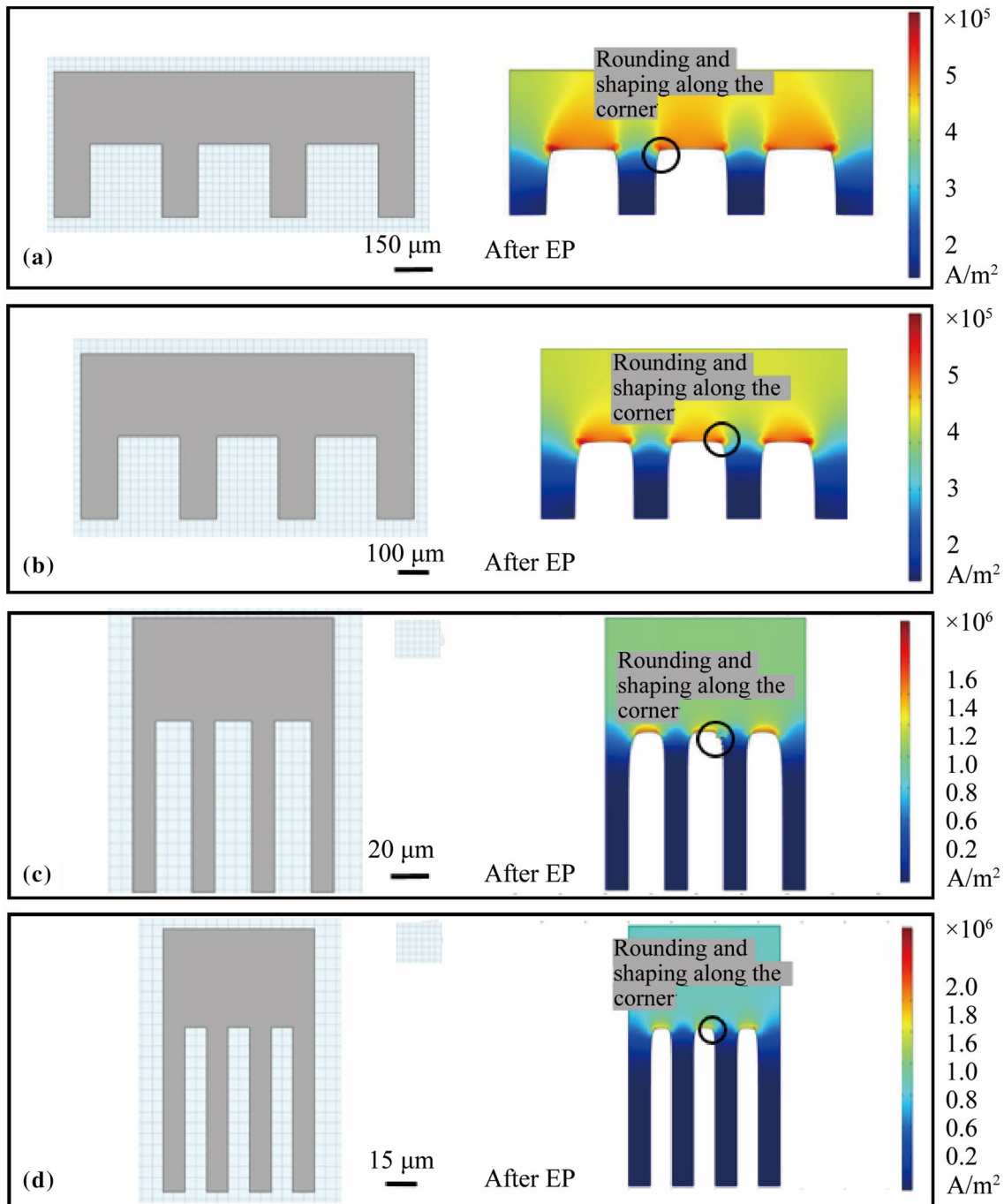
Fig. 15 SEM analysis of sample 3 with various ridges (R_1, R_2, R_3, R_4) **a–d** before electropolishing, and **e–h** after EP
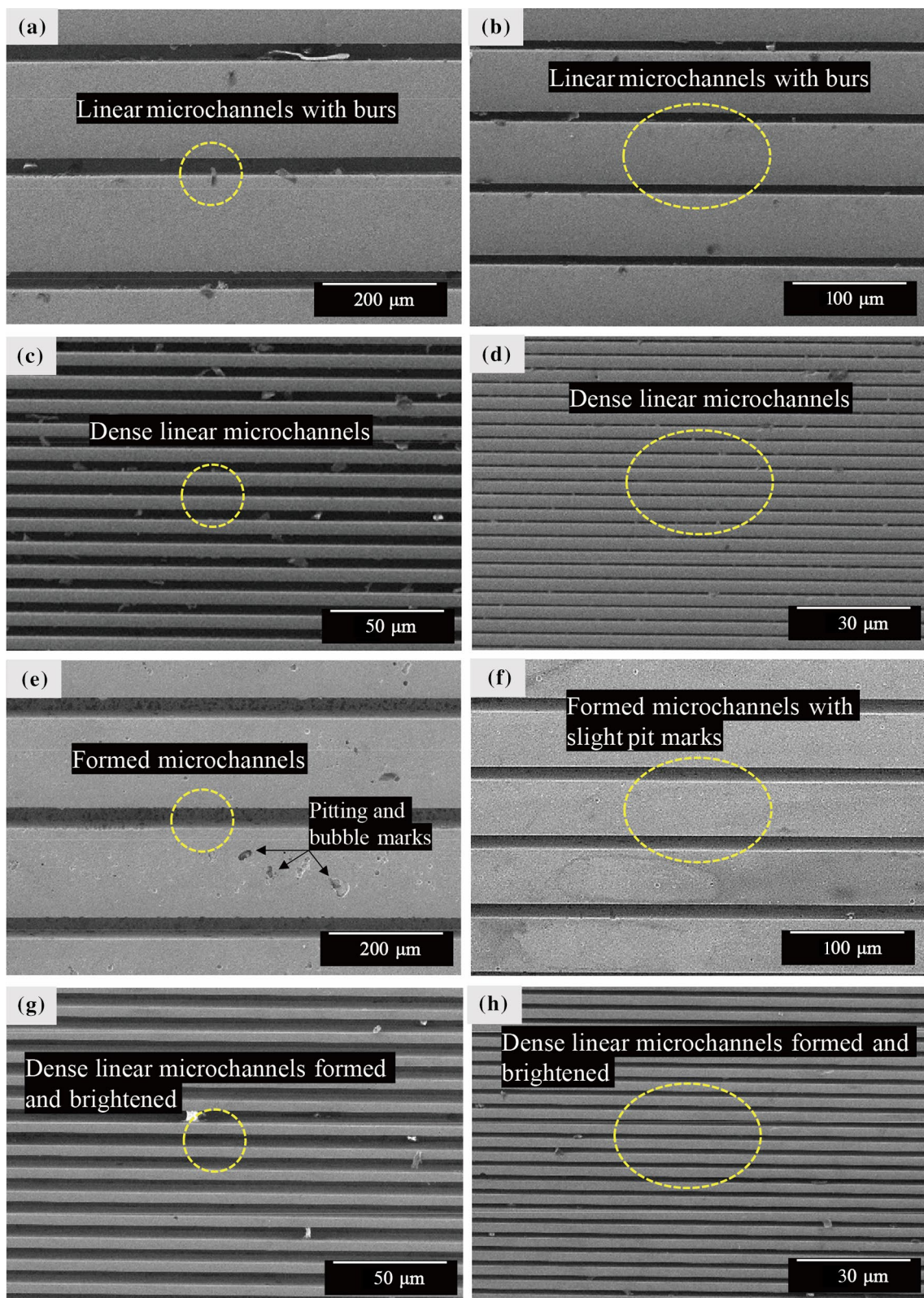
Fig. 16 SEM analysis of sample 4 **a**–**d** before EP, and **e**–**h** after EP

Fig. 17 Numerical simulation of Ni mould with multi-linear ridges using COMSOL, initial geometries and current density distribution after EP process (change in draft angle and fillet radius) **a** ridge 1 with width = 150 μm, height = 100 μm and gap = 50 μm, **b** ridge 2 with width = 90 μm, height = 100 μm and gap = 40 μm, **c** ridge 3 with width = 20 μm, height = 80 μm and gap = 15 μm, and **d** ridge 4 with width = 15 μm, height = 80 μm and gap = 20 μm

with longer EP times. To minimize bubble marks on the anode, increasing the circulation of electrolyte and maintaining a larger inter-electrode distance can be beneficial.

(ii) Quantitatively analysing the micro mould tools before and after EP indicated changes in the fillet radii, draft angle and surface roughness of the features. Increased time for EP led to more extensive shaping and forming of micro features. The star pattern samples that

were electropolished for 8 min (S_1) had an increased fillet radius of up to +3.58 μm, a positive change in draft angle of 2.16°–2.86° and an increase in surface roughness from 67.3 nm to 113 nm, while those electropolished for 15 min (S_2-1 and S_2-4) led to the fillet radius increasing from +3.76 μm to 4.73 μm, the establishment of a positive draft angle of 3.56°–3.62° and surface roughness increasing from 53 nm to 410 nm. For the multi-linear micro ridges that were electropolished for 8 min (sample 3), there was a similar increase in the fillet radius that was also of 2.45–3.7 μm, while the draft angle increased by 1.63°–2.18° and the surface roughness increased only slightly, from 20.3 nm to 31.4 nm. Finally, for the corresponding samples that were electropolished for 15 min (sample 4), the fillet radius increased by between 3.43 μm and 5.09 μm, the draft angle increased by 2.19°–3.58° and the surface roughness increased from 25.9 nm to 47.3 nm. There is a more pronounced change in fillet radius than in draft angle with prolonged EP times. These surface roughness values after EP are below 50 nm, which is typically required for mirror surface finishes. The increase in surface roughness, particularly for the shorter EP times, is not expected to prove significant in the optical transparency and effectiveness of the mould tools.

References

1. Zhang H, Zhang H, Guan T et al (2021) Prototyping and production of polymeric microfluidic chip. Adv Microfluid Nanofluid. https://doi.org/10.5772/intechopen.96355
2. Abdulhameed A, Halim MM, Halin IA (2023) Simulation and experimental validation of the interplay between dielectrophoretic and electroosmotic behavior of conductive and insulator particles for nanofabrication and lab-on-chip applications. Colloid Surface A 663:131065. https://doi.org/10.1016/j.colsurfa.2023.131065
3. Davis R, Singh A, Jackson MJ et al (2022) A comprehensive review on metallic implant biomaterials and their subtractive manufacturing. Int J Adv Manuf Tech 120(3/4):1473–1530
4. Wang X, Li C, Zhang Y et al (2022) Influence of texture shape and arrangement on nanofluid minimum quantity lubrication turning. Int J Adv Manuf Tech 119(1/2):631–646
5. Wang Y, Weng C, Deng Z et al (2023) Fabrication and performance of nickel-based composite mold inserts for micro-injection molding. Appl Surf Sci 615:156417. https://doi.org/10.1016/j.apsusc.2023.156417
6. Li J, Ma H, Liu W et al (2023) Effects of cavity thickness and mold surface roughness on the polymer flow during micro injection molding. Polymers 15(2):326. https://doi.org/10.3390/polym15020326
7. Moazzez B, O'Brien SM, Merschrod SEF (2013) Improved adhesion of gold thin films evaporated on polymer resin: applications for sensing surfaces and MEMS. Sensors 13(6):7021–7032
8. Chen J, Yang J, Zhou M et al (2021) Self-assembled monolayers of alkanethiols on nickel insert: characterization of friction and analysis on demolding quality in microinjection molding. Micromachines 12(6):636. https://doi.org/10.3390/mi12060636
9. Peixoto C, Valentim PT, Sousa PC et al (2022) Injection molding of high-precision optical lenses: a review. Precis Eng 76:29–51
10. Zhang N, Zhang H, Stallard C et al (2018) Replication integrity of micro features using variotherm and vacuum assisted microinjection moulding. CIRP J Manuf Sci Tec 23:20–38
11. Liarte E, Zambrano V, Gracia LA et al (2022) Demoulding process assessment of elastomers in micro-textured moulds. Open Res Europe 1:120. https://doi.org/10.12688/openreseurope.13716.2
12. Zariatin DL, Kiswanto G, Ko T (2017) Investigation of the micro-milling process of thin-wall features of aluminum alloy 1100. Int J Adv Manuf Tech 93:2625–2637
13. Raza S, Nadda R, Nirala C (2023) Real-time data acquisition and discharge pulse analysis in controlled RC circuit based micro-EDM. microsyst Technol 29(3):359–376
14. Arruebo M, Fernández-Pacheco R, Ibarra MR et al (2007) Magnetic nanoparticles for drug delivery. Nano Today 2(3):22–32
15. Schoenherr M, Ruehl H, Guenther T et al (2023) Adhesion-induced demolding forces of hard coated microstructures measured with a novel injection molding tool. Polymers 15(5):1285. https://doi.org/10.3390/polym15051285
16. Jong WR, Li TC, Chen YW et al (2017) Automatic recognition and construction of draft angle for injection mold design. Journal of Software Engineering and Applications (JSEA) 10(1):78–93
17. Łosiewicz B (2015) Electrodeposition mechanism of composite coatings. Solid State Phenom 228:65–78
18. Obilor AF, Pacella M, Wilson A et al (2022) Micro-texturing of polymer surfaces using lasers: a review. Int J Adv Manuf Tech 120(1/2):103–135
19. Lee H, Yi A, Choi J et al (2022) Texturing of polydimethylsiloxane surface for anti-reflective films with super-hydrophobicity in solar cell application. Appl Surf Sci 584:152625. https://doi.org/10.1016/j.apsusc.2022.152625
20. Ji JW, Khan MA, Zhan ZJ et al (2022) Electrochemical polishing of tungsten: an investigation of critical spatial frequency and ultimate roughness. J Electrochem Soc 169(4):043509. https://doi.org/10.1149/1945-7111/ac63fa
21. Li M, Chen Y, Luo W et al (2021) Demolding force dependence on mold surface modifications in UV nanoimprint lithography. Microelectron Eng 236:111470. https://doi.org/10.1016/j.mee.2020.111470
22. Kim SH, Asay DB, Dugger MT (2007) Nanotribology and MEMS. Nano Today 2(5):22–29
23. Chang WT, Hwang IS, Chang MT et al (2012) Method of electrochemical etching of tungsten tips with controllable profiles. Rev Sci Instrum 83:083704. https://doi.org/10.1063/1.4745394
24. Chen X, Yuan Q (2023) Capillary adhesion around the shapes optimized by dissolution. Adv Mater Interfaces 10(13):2202380. https://doi.org/10.1002/admi.202202380
25. Zaki S, Zhang N, Gilchrist MD (2022) Electropolishing and shaping of micro-scale metallic features. Micromachines 13(3):468. https://doi.org/10.3390/mi13030468
26. Li D, Zhang Y, Liu Y et al (2022) Injection moulding of mechanical micro-manufactured structures for optically encoding plastic surfaces. Opt Mater 123:111822. https://doi.org/10.1016/j.optmat.2021.111822
27. Zhang H, Zhang N, Fang F (2021) Investigation of mass transfer inside micro structures and its effect on replication accuracy in precision micro electroforming. Int J Mach Tool Manuf 165:103717. https://doi.org/10.1016/j.ijmachtools.2021.103717

28. Saitta L, Arcadio F, Celano G et al (2023) Design and manufacturing of a surface plasmon resonance sensor based on inkjet 3D printing for simultaneous measurements of refractive index and temperature. Int J Adv Manuf Tech 124(7/8):2261–2278

29. Zhang N, Liu J, Zhang H et al (2019) 3D printing of metallic microstructured mould using selective laser melting for injection moulding of plastic microfluidic devices. Micromachines 10(9):595. https://doi.org/10.3390/mi10090595

30. Martinho PG, Pouzada AS (2021) Alternative materials in moulding elements of hybrid moulds: structural integrity and tribological aspects. Int J Adv Manuf Tech 113(1):351–363

31. Shao L, Pan B, Hou R et al (2022) User-friendly microfluidic manufacturing of hydrogel microspheres with sharp needle. Biofabrication 14(2):025017. https://doi.org/10.1088/1758-5090/ac57a5

32. Bolat G, De la Paz E, Azeredo NF et al (2022) Wearable soft electrochemical microfluidic device integrated with iontophoresis for sweat biosensing. Anal Bioanal Chem 414(18):5411–5421

33. Li L, Li H, Kou G et al (2022) Dynamic camouflage characteristics of a thermal infrared film inspired by honeycomb structure. J Bionic Eng 19(2):458–470

34. Guan B, Pai JH, Cherrill M et al (2022) Injection moulding of micropillar arrays: a comparison of poly (methyl methacrylate) and cyclic olefin copolymer. Microsyst Technol 28:2083–2091

35. Chu Q, Wu A, Tan T et al (2021) Electropolishing behavior of niobium in choline chloride-based deep eutectic solvents. Appl Surf Sci 550:149322. https://doi.org/10.1016/j.apsusc.2021.149322

36. Kityk A, Protsenko V, Danilov F et al (2021) Enhancement of the surface characteristics of Ti-based biomedical alloy by electropolishing in environmentally friendly deep eutectic solvent (Ethaline). Colloid Surface A 613:126125. https://doi.org/10.1016/j.colsurfa.2020.126125

37. Jeong J, Yoon W, Chung B et al (2021) Fabrication of eco-friendly graphene nanoplatelet electrode for electropolishing and its properties. Appl Sci-basel 11(7):3224. https://doi.org/10.3390/app11073224

38. Kumar R (2019) MEMS based cantilever biosensors for cancer detection using potential bio-markers present in VOCs: a survey. Microsyst Technol 25(9):3253–3267

39. Pong-Ryol J, Tae-Sok J, Nam-Chol K et al (2016) Laser micropolishing for metallic surface using UV nano-second pulse laser and CW laser. Int J Adv Manuf Tech 85(9):2367–2375

40. Yang B, Ai Y (2022) Facile fabrication of CuO nanosheets and in situ transmission electron microscopy/X-ray diffraction heating characterization of microstructure evolution. Phys Status Solidi A 219(6):2100617. https://doi.org/10.1002/pssa.202100617

41. Shen H, Liao C, Zhou J et al (2021) Two-step laser based surface treatments of laser metal deposition manufactured Ti6Al4V components. J Manuf Process 64:239–252

42. Du L, Guo B, Dong Y et al (2022) A wearable omnidirectional inertial switch of security detection for the elderly. Microsyst Technol 28:2011–2021

43. Zhao Y, Qian S, Zhang Y et al (2021) Experimental study on uniformity of copper layer with microstructure arrays by electroforming. Int J Adv Manuf Tech 114(7):2019–2030

44. Zaki S, Zhang N, Gilchrist MD (2022) Potentiodynamic polarization behaviour of Ni for shaping and electropolishing of micromould tools. In: Proceedings of the 38th international manufacturing conference (IMC38), University College Dublin, Dublin

45. Paul R, Hackert-Oschätzchen M, Danilov I et al (2019) 3D multiphysics simulation of jet electrochemical machining of intersecting line removals. Procedia CIRP 82:196–201

Sana Zaki Ph.D. student (Mechanical Engineering). University College Dublin.

Nan Zhang Associate Professor of Polymer Manufacturing, University College Dublin.

Michael D. Gilchrist Full Professor of Mechanical Engineering, UCD.